

# A Simple Broadband Flat-Gain Circularly Polarized Aperture Antenna with Multiple Radiation Modes

Yi-Xuan Zhang<sup>\*</sup>, Yong-Chang Jiao, Huan Zhang, and Yang Gao

**Abstract**—A simple broadband circularly polarized (CP) aperture antenna is proposed in this paper. The antenna is composed of an L-shaped feed line and a circular aperture. With the newly introduced perturbation slots, a new resonant mode  $TE_{31}$  is generated, which can widen the CP bandwidth without increasing the antenna size. Measured results of the fabricated antenna shows 93.5% (2.9–8 GHz) impedance bandwidth ( $|S_{11}| < -10$  dB) and 66.6% (3–6 GHz) 3 dB axial-ratio bandwidth. The overlapped CP working band covers the entire WiMAX, WLAN and lower frequency 5G bands. Its peak gain is 4.9 dBic at 3.5 GHz, and its gain variation is less than 1 dBic within 3–5.8 GHz band. Design considerations, empirical formulas and surface current analysis are also presented and discussed.

## 1. INTRODUCTION

Nowadays, circularly polarized (CP) antennas have attracted much attention in many wireless systems such as satellite communication system, wireless local area network (WLAN) system, and worldwide interoperability for microwave access (WiMAX) system. The development of broadband CP antennas is becoming more and more important due to the increasing demands for higher data rate and more capacity in modern wireless systems [1–3]. By using broadband CP antennas, not only the multipath effects can be mitigated, but also the complexity inherent in the multiservice wireless systems can be reduced. In recent years, many broadband CP antennas have been proposed [4–19]. Among them, wide apertures with single feed structure have been widely studied, owing to their features such as wide impedance bandwidth, low cost low profile, and easy fabrication. However, most of them have limited 3 dB axial-ratio (AR) bandwidth. Several methods were proposed to overcome this problem. In [4] and [5], the parasitic loading technique was introduced to improve the AR bandwidth, resulting in 3 dB AR bandwidths of 45% and 56%, respectively. However, the introduced parasitic structure greatly increases the antenna profile and design complicity. Semicircular patch was also employed to obtain wide 3 dB AR bandwidth (49.8% and 58.7% respectively) [6, 7]. However, the gain variation is more than 2 dBic within the obtained CP band, and the 1 dBic gain variation bandwidth is relatively narrow.

In this paper, a simple broadband CP antenna with flat gains is proposed. The antenna covers the entire 3.5 GHz WiMAX, 5.2/5.8 GHz WLAN and 3.5/4.9 GHz lower frequency 5G bands with gain variation less than 1 dBic. Based on the mode analysis, two original CP modes are produced by the L-shaped feed line and the circular aperture. The perturbation slots are introduced to adjust the surface current distributions on the ground plane, and to generate a new resonant mode at the higher frequency band, thus the 3 dB AR bandwidth is obviously improved. To better explain the working principle of the perturbation slots, the surface current distributions and performance comparison are studied. Design considerations and empirical formulas are also given to provide better understanding of antenna working mechanism and fast estimation of initial dimensions.

---

Received 7 November 2017, Accepted 18 January 2018, Scheduled 25 January 2018

<sup>\*</sup> Corresponding author: Yi-Xuan Zhang (yxuzhang@foxmail.com).

The authors are with the National Key Laboratory of Antennas and Microwave Technology, Xidian University, Xi'an 710071, P. R. China.

## 2. ANTENNA DESIGN AND ANALYSIS

Figure 1 shows the configuration of the proposed broadband CP antenna. The antenna is fabricated on an FR4 substrate (thickness  $h = 1.2$  mm and relative permittivity  $\epsilon_r = 4.4$ ). A circular aperture with radius  $R_a = 58.8$  mm is etched on the ground plane, while a pair of perturbation slots with length  $L_s$  and width  $W_s$  is etched at the edge of the circular aperture. The L-shaped feed line is etched on the other side of the substrate. The tapered part of the feed line (with length  $L_t$ ) and the microstrip line (with width  $W_m$ ) are used to match the  $50\ \Omega$  input impedance. A round structure on the corner of the L-shaped feed line is also introduced to improve the flat gain characteristic.

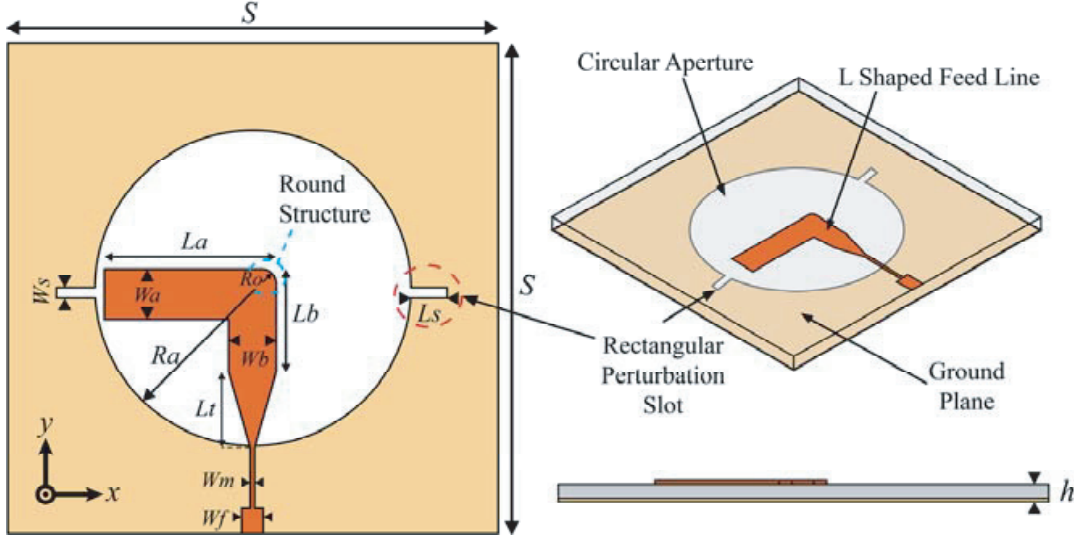


**Figure 1.** Configuration of the proposed antenna.

The vertical and horizontal parts of the L-shaped feed line are used to produce two orthogonal electric fields at boresight. When the two orthogonal electric fields have nearly same magnitude and near  $90^\circ$  phase difference, good CP results can be obtained. Thus, the electrical length of the horizontal part is set to about  $90^\circ$  to make the current phase on the horizontal part  $90^\circ$  lag behind that of the vertical part [8]. To better understand the CP radiation of the proposed antenna, the unbalances of magnitudes and phase difference between  $E_x$  and  $E_y$  (obtained at boresight) are presented in Figure 2. As shown in the figure, the two orthogonal electric fields have nearly same magnitude and near  $90^\circ$  phase difference in the desired frequency band, which verifies the CP radiation of the proposed antenna at boresight.

The way for widening the CP bandwidth of the proposed antenna is to generate more efficient radiation modes. When all the efficient radiation modes are evenly distributed within a frequency band, and these modes can be excited at the same time, wide CP bandwidth can be obtained. For the proposed antenna structure without the perturbation slots, its circularly polarized resonant modes are  $TE_{11}$  and  $TE_{21}$  [9]. The resonant frequency of each mode can be determined by the empirical formula

$$f_{TE_{m1}} = \frac{A_{m1}c}{C_a} \times \left( \frac{1 + \epsilon_r}{2\epsilon_r} \right)^{\frac{1}{2}}, \quad m = 1, 2, 3 \quad (1)$$

where  $c$  is  $3 \times 10^8$  m/s, and  $\epsilon_r$  represents the relative permittivity of the substrate.  $C_a$  is the circumference of the aperture, and  $A_{m1}$  is the coefficient corresponding to mode  $TE_{m1}$ , where the estimated  $A_{11}$ ,  $A_{21}$  and  $A_{31}$  are 1.84, 3.05 and 4.2, respectively. By adding a pair of rectangular perturbation slots in the circular aperture, a new AR minimum point (corresponding to mode  $TE_{31}$ ) is produced at the higher frequency band. By tuning the parameters properly, these three resonant points merge and form a wider 3 dB AR band, and thus the obtained CP bandwidth increases from 44% to 66% without increasing the antenna size or introducing extra element. Table 1 shows the final design parameters of the proposed antenna.

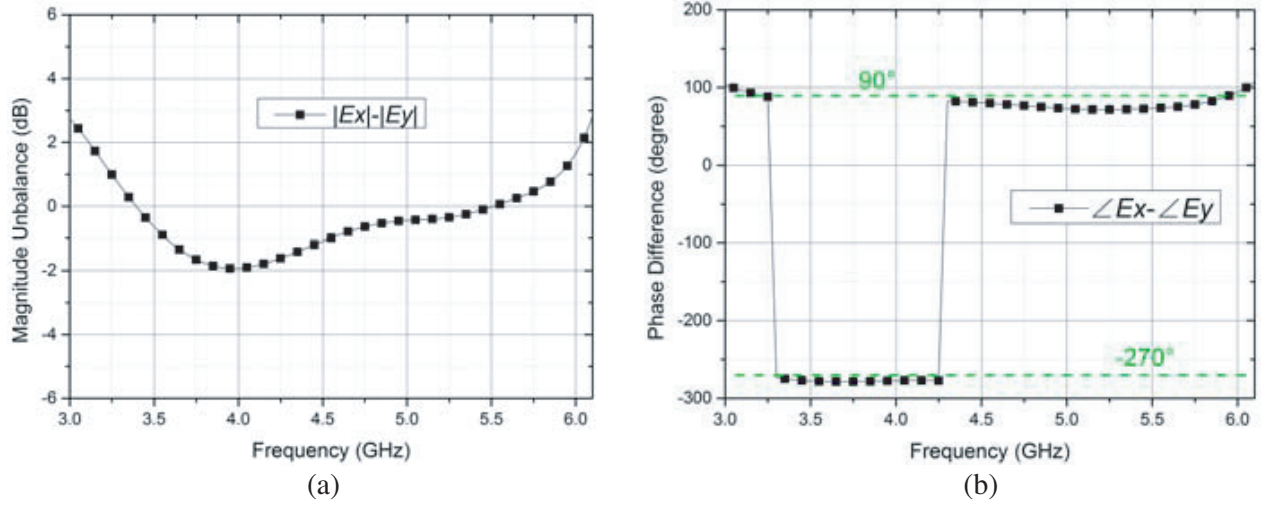


**Figure 2.** Relationships of the radiated orthogonal electric fields at boresight. (a) Unbalance of magnitude. (b) Phase difference.

**Table 1.** Parameters of the proposed antenna (units: mm).

$S$	$h$	$Ra$	$Wa$	$La$	$Wb$	$Lb$	$Lt$	$Wm$	$Wf$	$Ws$	$Ls$	$Ro$
58.8	1.2	19.3	5.9	15	5.7	13.8	9.9	0.6	1.9	1.4	5.88	2

### 2.1. Effects of the Perturbation Slots

The mathematical and physical explanations of the working principle of the perturbation slots are discussed in this subsection. When antenna structure is without the perturbation slots, it has two resonant modes  $TE_{11}$  and  $TE_{21}$  [9]. In this case, Eq. (1) can also be written as

$$f_{TE_{m1}} = \frac{A_{m1}c}{2\pi Ra} \times \left( \frac{1 + \epsilon_r}{2\epsilon_r} \right)^{\frac{1}{2}}, \quad m = 1, 2, 3 \quad (2)$$

Here,  $Ra$  is the radius of the circular aperture, and the calculated  $TE_{11}$  and  $TE_{21}$  resonance frequencies are 3.6 and 5.9 GHz, which correspond well to the simulated  $|S_{11}|$  minimum points in Figure 3(a).

If the perturbation slots are introduced, Eq. (1) should be written as

$$\begin{cases} f_{TE_{m1}} = \frac{A_{m1}c}{2\pi Ra} \times \left( \frac{1 + \epsilon_r}{2\epsilon_r} \right)^{\frac{1}{2}}, & m = 1 \\ f_{TE_{m1}} = \frac{A_{m1}c}{2\pi Ra + 2Ls} \times \left( \frac{1 + \epsilon_r}{2\epsilon_r} \right)^{\frac{1}{2}}, & m = 2, 3 \end{cases} \quad (3)$$

where  $Ls$  is the length of the perturbation slots, and the modifications in the second formula represent the extended current path caused by the perturbation slots. The calculated resonance frequencies by Eq. (3) are 3.6, 5.4 and 7.4 GHz for  $TE_{11}$ ,  $TE_{21}$  and  $TE_{31}$  mode, and the results correspond well to the simulated one in Figure 3(a). The formula for  $TE_{11}$  mode is not changed here, which is mainly because compared with the  $TE_{11}$  mode wavelength, the width of the slots  $Ws$  is relatively small, thus has little influence on the  $TE_{11}$  mode.

Based on the mathematical interpretation, a physical explanation can be concluded that with the perturbation slots, the current path of  $TE_{21}$  and  $TE_{31}$  modes can be extended while having little influence on the behavior of  $TE_{11}$ . Under this condition, the resonance frequencies of  $TE_{21}$  and  $TE_{31}$  modes can be reduced, while keeping  $TE_{11}$  resonance frequency almost stable. With proper tuning the resonant points of three modes can merge, thus a wider CP bandwidth can be obtained.

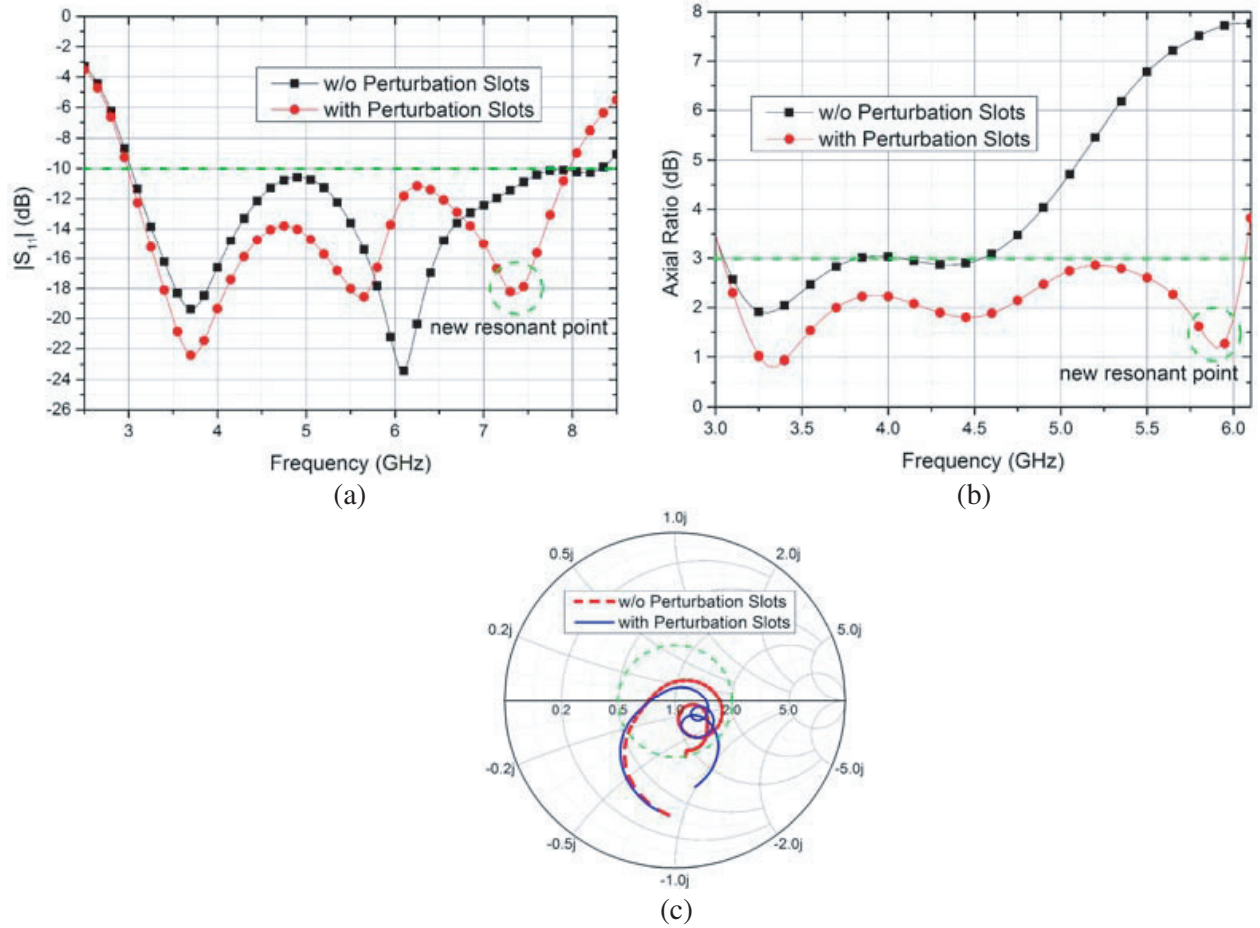


**Figure 3.** Simulated results of the antennas with and without the perturbation slots. (a)  $|S_{11}|$ . (b) AR. (c) Smith Chart.

Simulated  $|S_{11}|$  and AR results of the antennas with and without the perturbation slots are compared in Figures 3(a) and 3(b), respectively. As shown in the figures, a new AR resonant point at the higher frequency band is successfully introduced by the perturbation slots, and the proposed antenna has three minimum AR points, comparing only two minimum AR points for the antenna without the perturbation slots in [9]. This can also be illustrated by the simulated Smith Chart in Figure 3(c). Obviously, by introducing the perturbation slots, a new small loop occurs in the impedance loci, which produces a new CP operating point. To verify the CP radiations of these three resonant modes, the current distributions at different time phases are studied, as shown in Figure 4. The vector sum of the dominant current rotates anticlockwise as time phase increases, which can generate right-hand CP (RHCP) waves in  $+z$  direction.

To better demonstrate how the perturbation slots influence the antenna performance, the simulated current distributions of the antenna structure with and without the perturbation slots are compared in Figure 5. Major differences are marked with Circles 1, 2, 3, and 4. As shown in Circle 1, with the perturbation slots, the current distributions on the left and right edges of the aperture become relatively uniform. Circles 2, 3 and 4 indicate that the surface current orientations of some parts in the ground plane are approximately inverted, due to the perturbation slots. With this inverting phenomenon, the current distributions on the left and right sides of the ground plane become nearly symmetric, which is beneficial for generating a resonant mode around this frequency. Moreover, from the current trace marked as 5 in Figure 5, the perturbation slots fold the current trace at the edge of the circular aperture. This folded current distribution forms an extended current path, which is helpful for generating a higher order mode.

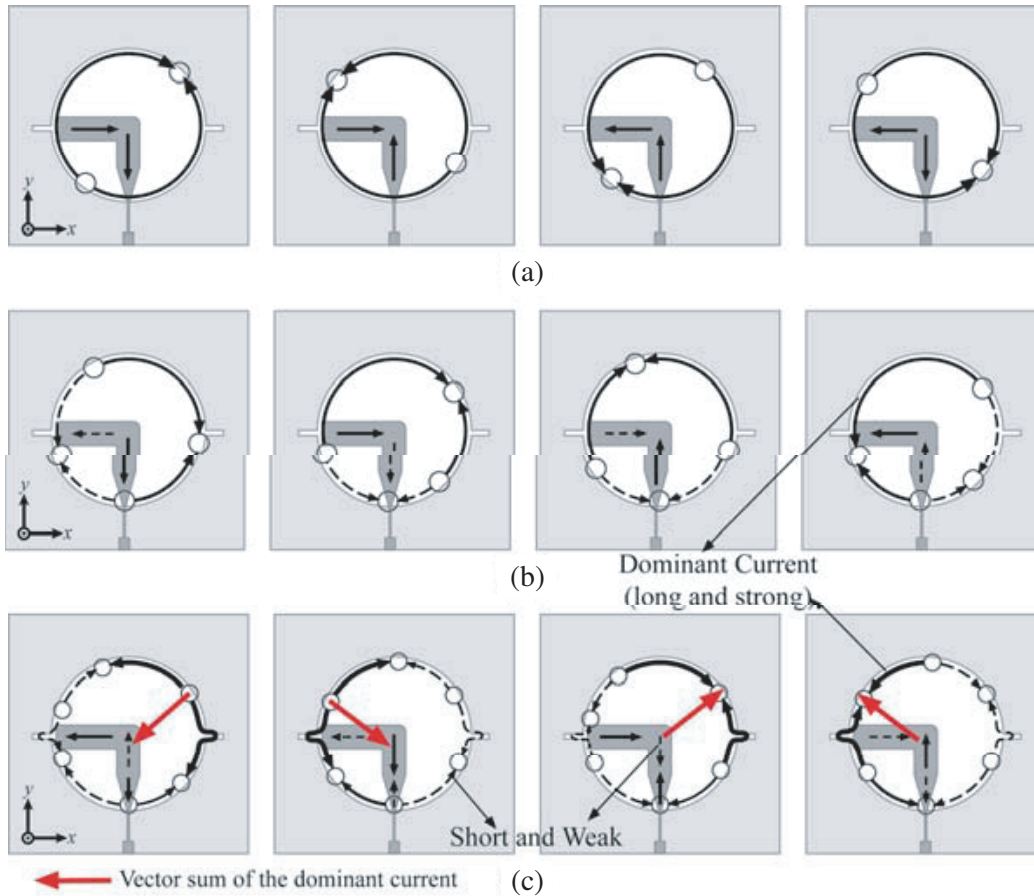


**Figure 4.** Current distributions at different time phases of 0°, 90°, 180° and 270° from left to right. (a) 3.3 GHz (TE<sub>11</sub>). (b) 4.5 GHz (TE<sub>21</sub>). (c) 5.9 GHz (TE<sub>31</sub>).

Figure 6 shows influences of the dimensions of the perturbation slots on the  $|S_{11}|$  and AR results. By tuning the parameters properly, a new resonant point can be generated, as shown in curves 2, 3 and 4 in Figure 6. Finally, by choosing appropriate resonant frequency, a wider CP band is obtained, as shown in curve 2 in Figure 6.

### 2.2. Effect of the Round Structure on Flat Gains

Figure 7 shows the simulated results of the antennas with and without the round structure. From Figure 7(a), with the round structure, the antenna gains become flat in the CP operating band. The 1 dBic gain variation band covers the entire 3.5 GHz WiMAX and 5.2/5.8 GHz WLAN bands, which provides a broad operating band for stable CP wave radiation. From Figure 7(b), the round structure may also slightly affect the AR results of the antenna, but the obtained 3 dB AR bandwidth is almost unchanged.

## 3. EXPERIMENTAL RESULTS

The simulated and measured  $|S_{11}|$  and AR results are presented in Figure 8. The measured impedance band is 2.9–8 GHz (94% centered at 5.4 GHz), and the measured AR bandwidth is 3–6 GHz (66.6% centered at 4.5 GHz). The discrepancies between the measured and simulated results are mainly caused by the nonuniform parameters of the substrate, fabrication tolerances and chamber mounting. Figure 9 shows the radiation patterns at 3.3 and 5.8 GHz. The radiated CP wave in +z direction is RHCP wave,

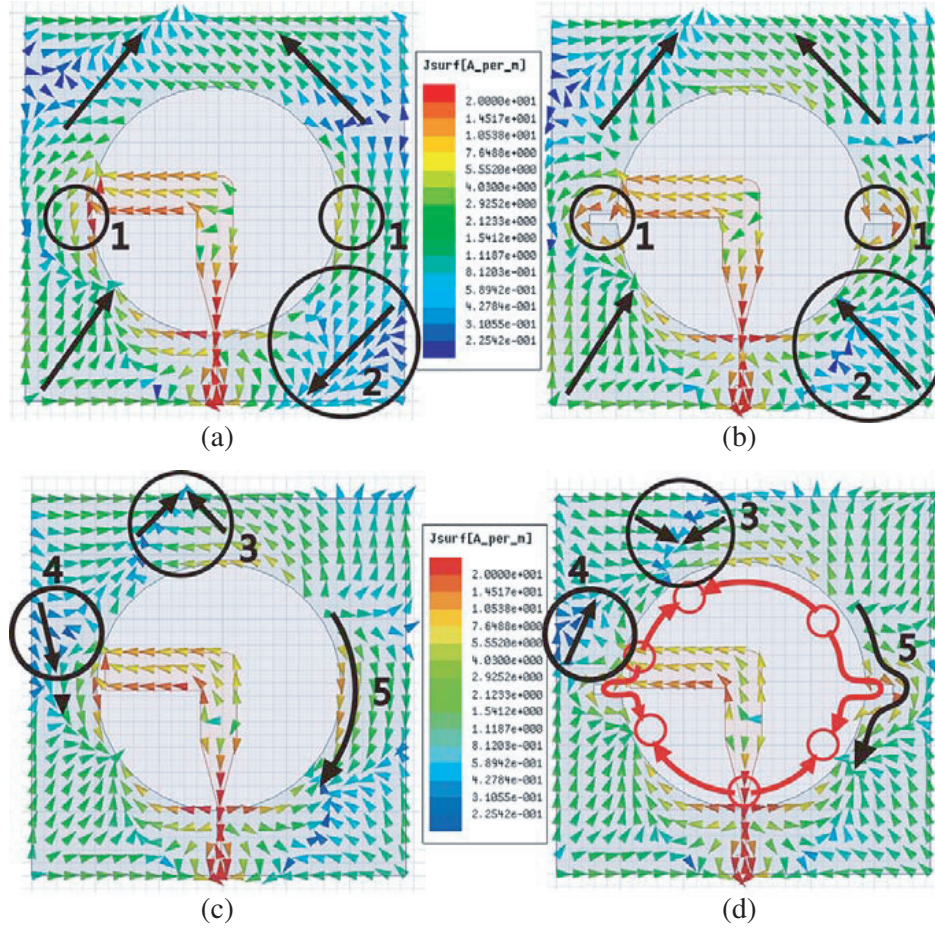


**Figure 5.** Effects of the perturbation slots on the surface current distributions. (a) Without perturbation slots at 5.5 GHz. (b) With perturbation slots at 5.5 GHz. (c) Without perturbation slots at 5.9 GHz. (d) With perturbation slots at 5.9 GHz.

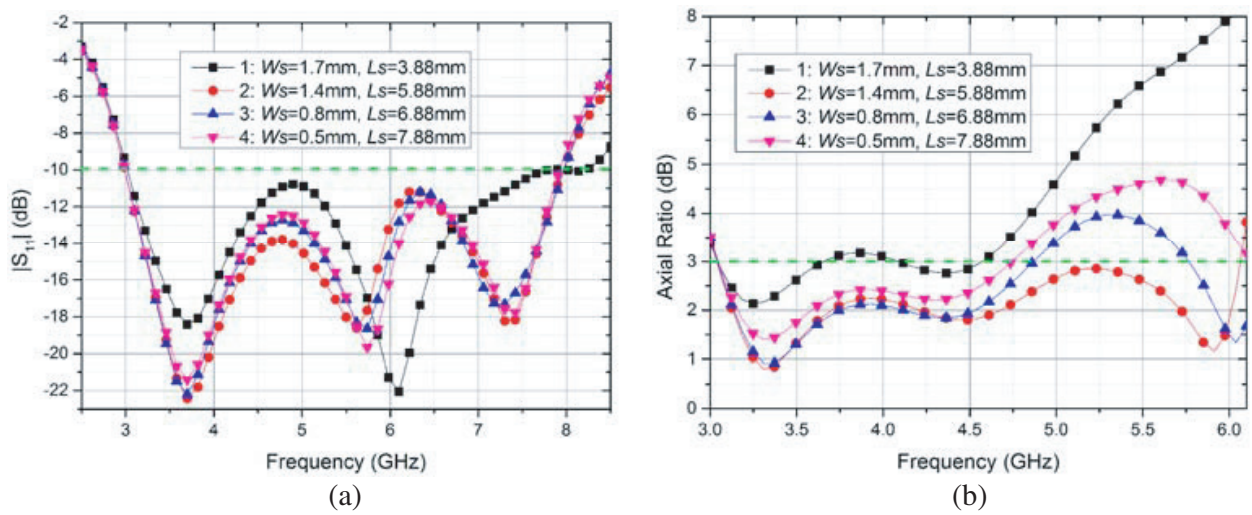


**Figure 6.** Simulated results for different combinations of  $W_s$  and  $L_s$ . (a)  $|S_{11}|$ . (b) AR.

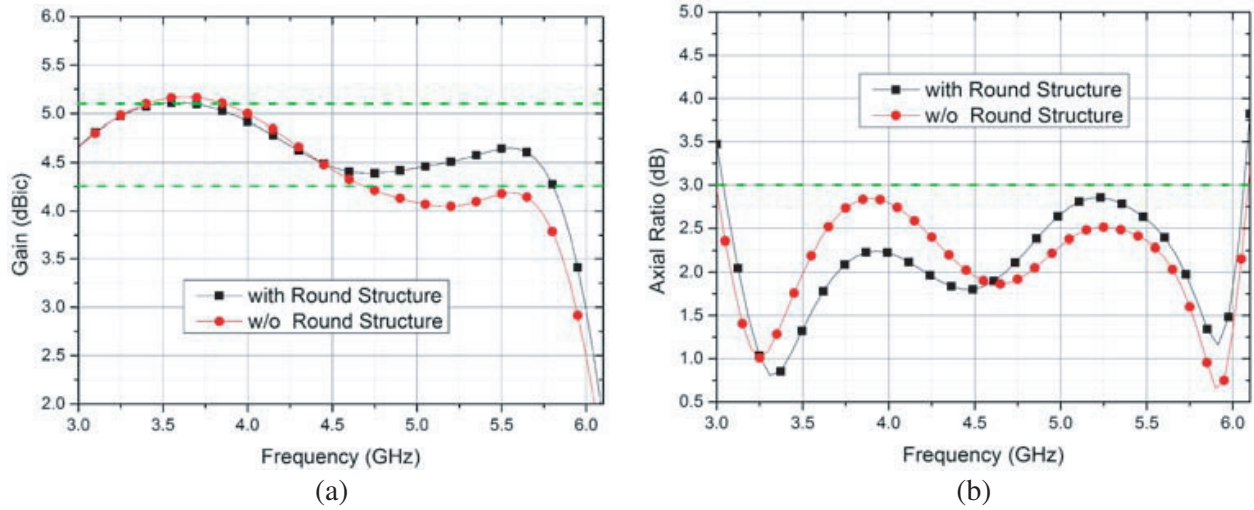


**Figure 7.** Simulated results for the antennas with and without the round structure. (a) Antenna gains. (b) AR.

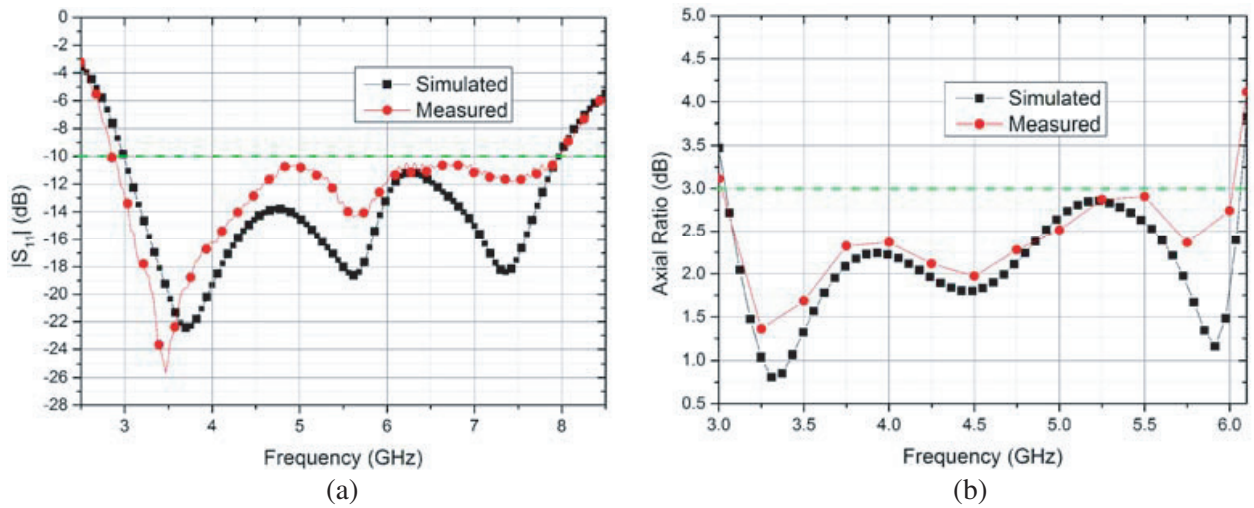


**Figure 8.** Simulated and measured results for the proposed antenna. (a)  $|S_{11}|$ . (b) AR.

**Table 2.** Comparison of the proposed antenna with other existing broadband CP antennas.

Referenced Antenna	Impedance Bandwidth	AR Bandwidth	1 dBic gain bandwidth
[4]	45%	45%	45%
[5]	60%	56%	56%
[6]	101%	49.8%	< 27%
[7]	111.6%	58.4%	< 25%
[10]	38%	44%	~ 44%
[11]	60%	62%	NA
[12]	76.9%	44.9%	44.9%
[13]	63.4%	57.4%	< 45%
This work	93.5%	66.6%%	63.6%

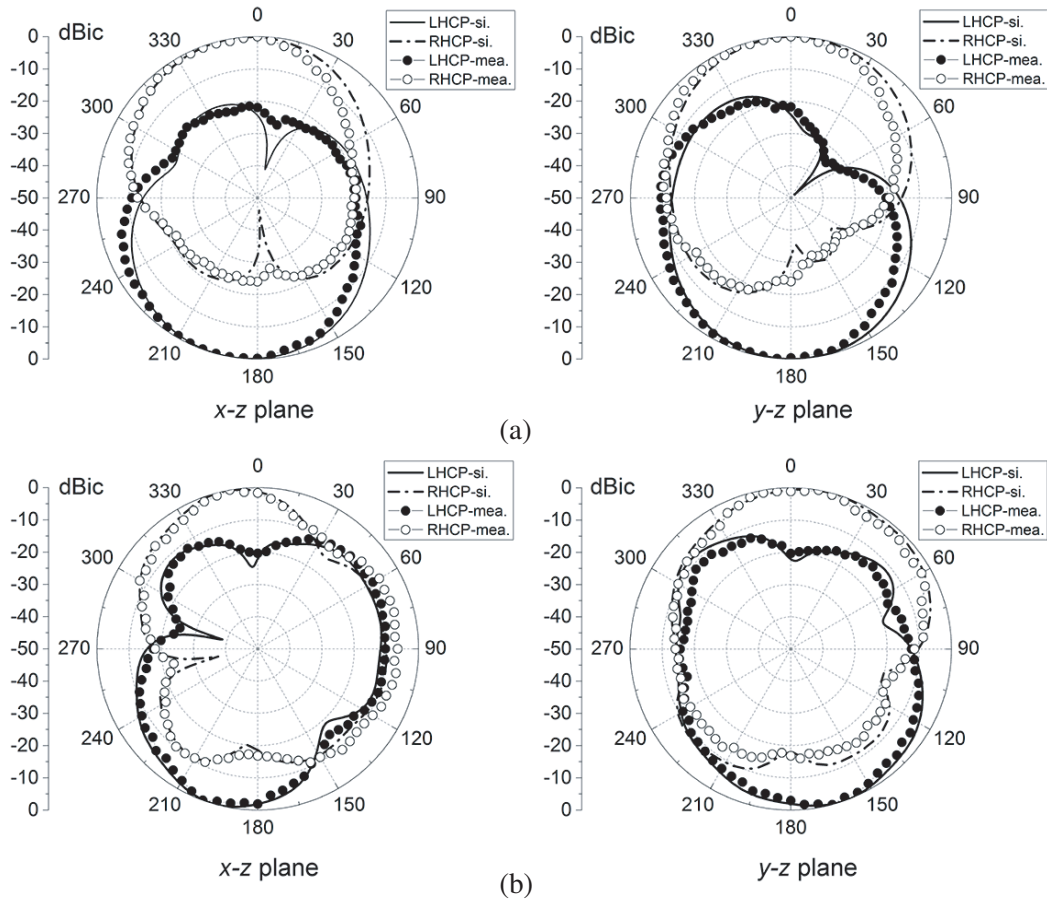


**Figure 9.** Simulated and measured radiation patterns for the proposed antenna. (a) 3.3 GHz. (b) 5.8 GHz.

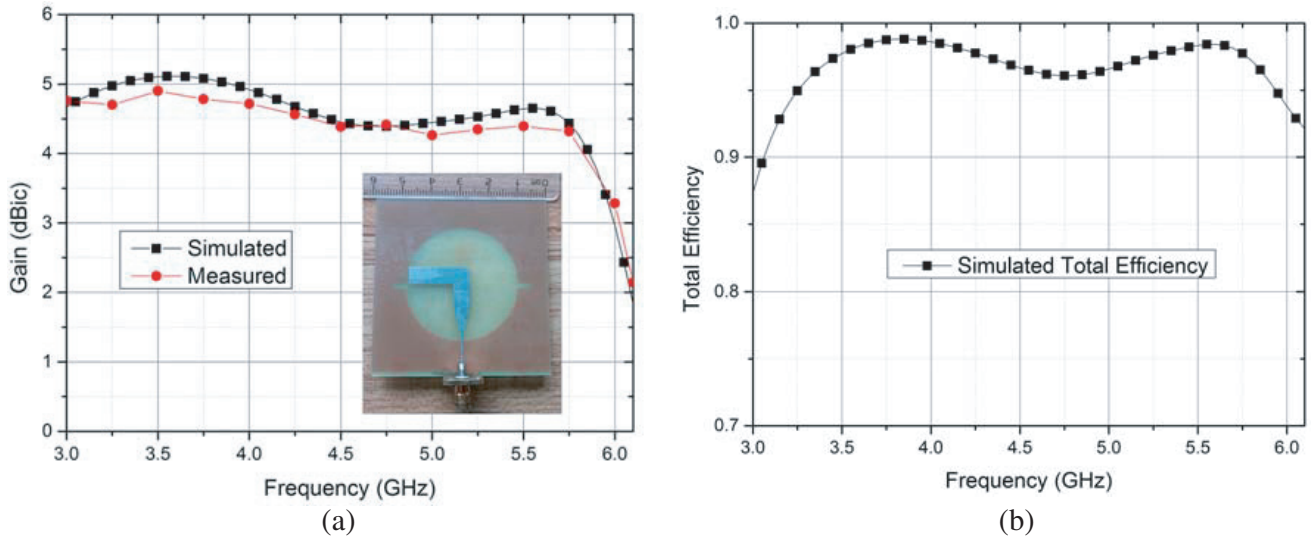


**Figure 10.** Simulated and measured results of the proposed antenna. (a) Simulated and measured antenna gains. (b) Simulated total efficiency.

while in the  $-z$  direction it is left-hand CP (LHCP) wave. From the antenna radiation patterns, the main beam is tilted away from boresight direction, which is mainly caused by the asymmetric feeding structure of the proposed aperture antenna. To solve his problem, the proposed antenna can be extended into an array with special designed array arrangement, which will be discussed in our following work.

Figure 10(a) plots simulated and measured gains in  $+z$  direction. As shown in the figure, measured gains with maximum variation less than 1 dBic are obtained from 3 to 5.8 GHz, which means a flat gain bandwidth of 63.6% (center frequency 4.4 GHz). The measured peak gain is 4.9 dBic at 3.5 GHz. Figure 10(b) shows the simulated total efficiency of the proposed antenna which has a total efficiency above 87% in its CP working band. Table 2 shows the comparison of the proposed antenna with other broadband CP antennas. Obviously, the proposed antenna has wider CP and flat gain bandwidths. Thus, the proposed antenna is an attractive candidate for multi-service wireless systems which covers WiMAX, WLAN and low frequency 5G band.

#### 4. CONCLUSIONS

This paper presents a simple broadband CP antenna with flat gains, which covers entire WiMAX, WLAN and lower frequency 5G bands. The antenna is composed by an L-shaped feed line and a circular aperture with a pair of rectangular perturbation slots. Besides the  $TE_{11}$  and  $TE_{21}$  CP modes inherently produced by the circular aperture, a new CP mode  $TE_{31}$  is introduced by the perturbation slots at 5.9 GHz. Owing to the new resonant mode, a wide useable CP band ranging from 3 to 6 GHz is obtained. Moreover, the proposed antenna also has flat-gain characteristic, and its 1 dBic gain variation band is 3–5.8 GHz. Design considerations, empirical formulas and surface current analysis are also presented and discussed.

#### ACKNOWLEDGMENT

This work is supported in part by the National Key R&D Program of China under Grant 2017YFB0202102.

#### REFERENCES

1. Yang, S. S., K.-F. Lee, A. A. Kishk, and K.-M. Luk, "Design and study of wideband single feed circularly polarized microstrip antennas," *Progress In Electromagnetics Research*, Vol. 80, 45–61, 2008.
2. Mohammadi, P. and V. Rafii, "High gain and broadband circularly polarized square slot antenna array," *Progress In Electromagnetics Research Letters*, Vol. 43, 105–113, 2013.
3. Xu, P., Z.-H. Yan, T.-L. Zhang, and X.-Q. Yang, "Broadband circularly polarized slot antenna array with Fan-shaped feed line and L-shaped grounded strips," *Progress In Electromagnetics Research Letters*, Vol. 44, 125–131, 2014.
4. Row, J.-S. and S.-W. Wu, "Circularly-polarized wide slot antenna loaded with a parasitic patch," *IEEE Trans. Antennas Propag.*, Vol. 56, No. 9, 2826–2832, 2008.
5. Zhang, H., Y.-C. Jiao, L. Lu, and C. Zhang, "Broadband circularly polarized square-ring-loaded slot Antenna with flat gains," *Antennas Wireless Propag. Lett.*, Vol. 16, 29–32, 2017.
6. Le, T. T. and H. C. Park, "Very simple circularly polarised printed patch antenna with enhanced bandwidth," *Electron Lett.*, Vol. 50, 1896–1898, 2014.
7. Le, T. T., V. H. The, and H. C. Park, "Simple and compact slot-patch antenna with broadband circularly polarized radiation," *Microwave Opt. Technol. Lett.*, Vol. 58, No. 7, 1634–1641, 2016.
8. Yeung, S. H., K. F. Man, and W. S. Chan, "A bandwidth improved circular polarized slot antenna using a slot composed of multiple circular sectors," *IEEE Trans. Antennas Propag.*, Vol. 59, No. 8, 3065–3070, 2011.
9. Yang, W. and J. Zhou, "Wideband circularly polarized cavity-backed aperture antenna with a parasitic square patch," *Antennas Wireless Propag. Lett.*, Vol. 13, 197–200, 2014.

10. Tseng, L. Y. and T. Y. Han, "Microstrip-fed circular slot antenna for circular polarization," *Microwave Opt. Technol. Lett.*, Vol. 50, No. 4, 1056–1058, 2008.
11. Panahi, A., X. L. Bao, G. Ruvio, and M. J. Ammann, "A printed triangular monopole with wideband circular polarization," *IEEE Trans. Antennas Propag.*, Vol. 63, No. 1, 415–418, 2014.
12. Zhang, L., Y. C. Jiao, Y. Ding, B. Chen, and Z. B. Weng, "CPW-fed broadband circularly polarized planar monopole antenna with improved ground-plane structure," *IEEE Trans. Antennas Propag.*, Vol. 61, No. 9, 4824–4828, 2013.
13. Li, G., H. Zhai, T. Li, L. Li, and C. Liang, "CPW-fed S-shaped slot antenna for broadband circular polarization," *Antennas Wireless Propag. Lett.*, Vol. 12, 619–622, 2013.
14. Simruni, M. and S. Jam, "A circularly-polarized compact wideband patch antenna loaded by metamaterial structures," *Progress In Electromagnetics Research C*, Vol. 78, 93–104, 2017.
15. Deng, J., L. Guo, T. Fan, Z. Wu, Y. Hu, and J. Yang, "Wideband circularly polarized suspended patch antenna with indented edge and gapcoupled feed," *Progress In Electromagnetics Research*, Vol. 135, 151–159, 2013.
16. Zhang, L., Y.-C. Jiao, and Z.-B. Weng, "Wideband circularly polarized dielectric resonator antenna with a square spiral microstrip feedline," *Progress In Electromagnetics Research Letters*, Vol. 41, 11–20, 2013.
17. Chen, Q., H.-L. Zheng, T. Quan, and X. Li, "Broadband CPW-fed circularly polarized antenna with equiangular tapered-shaped feedline for ultra-wideband applications," *Progress In Electromagnetics Research C*, Vol. 26, 83–95, 2012.
18. Lin, F. H., Z. N. Chen, and W. Liu, "A metamaterial-based broadband circularly polarized aperture-fed grid-slotted patch antenna," *Proc. IEEE Asia-Pacific Conf. Antennas Propag. (APCAP)*, 353–354, Kuta, Indonesia, 2015.
19. Ellis, M. S., J. J. Kponyo, and A.-R. Ahmed, "A compact wideband circularly polarized L-slot antenna edge-fed by a microstrip feedline for C-band applications," *Progress In Electromagnetics Research Letters*, Vol. 65, 95–102, 2017.